1

Assignment IV Leaky Waves

EE4620 Spectral Domain Methods in Electromagnetics

Petar V. Peshev, p.v.peshev@student.tudelft.nl
Department of Electrical Engineering, Mathematics, and Computer Science,
Delft University of Technology, Delft, The Netherlands

Abstract

In this assignment, the propagation constant of the TM1 and TE1 leaky wave modes is calculated in superstrate and semi-infinite superstrate, as a function of frequency and permittivity. Furthermore, the directivity and bandwidth of a Fabry-Parot antenna in these stratifications are also investigated. Finally, the TM0 propagation constant in semi-infinite superstrate is investigated, and double slot antenna is designed to cancel the TM0 mode; the radiation pattern of the double slot antenna with semi-infinite stratification is compared to the pattern of a single slot antenna.

I. SIMULATIONS

The scripts of this assignment are in the GIT repository Assignment IV; and the library developed and used in the scripts is in spectral-methods-library. To run the simulations either place the script and library repositories in the same parent folder or change the library path in the simulation scripts.

II. SUPERSTRATE

In a superstrate stratification, the dispersion equation is

$$D(k_\rho) = Z_L + j\zeta_0 \tan(k_{z0}h), \tag{1}$$

where ζ_0 and k_{z0} are the wave impedance and z-component of the wave vector in free space respectively, h the free space height, and Z_L the input impedance seen from the first free space to dielectric interface and is

$$Z_L = \zeta_d \frac{\zeta_0 + j\zeta_d \tan(k_{zd}h_s)}{\zeta_d + j\zeta_0 \tan(k_{zd}h_s)}, \tag{2}$$

where ζ_d and k_{zd} are the wave impedance and z-component of the wave vector in the dielectric respectively, and h_s the dielectric height. Moreover, the z-component of the wave vector in the dispersion equation is

$$k_{z0} = j\sqrt{-k_0^2 + k_\rho^2}, \tag{3}$$

due to the poles being located in the bottom Riemann sheet and $k_\rho = \sqrt{k_x^2 + k_y^2}$ is the ρ-component of the wave vector in cylindrical coordinates.

Finally, the approximated solutions to the dispersion equation for the TE1 and TM1 modes are

$$k_{z0}^{TE} \approx \frac{k_0}{\pi\epsilon_r(2\bar{h})^2}\frac{2\pi\bar{h}\epsilon_r + j}{1 + \frac{1}{(2\pi\bar{h}\epsilon_r)^2}}, \tag{4a}$$

$$k_{z0}^{TM} \approx \frac{k_0}{4\bar{h}}(1 + \sqrt{1 + 8j\frac{\bar{h}}{\pi\epsilon_r}}), \tag{4b}$$

where $\bar{h} = h/\lambda_0$. In the derivation of the approximate solutions, the ρ-component of the wave vector is taken to be zero $k_\rho = 0$, consequently, $Z_L = \zeta_0/\epsilon_r$.

The normalized to k_0 propagation constant of the TM1 and TE1 modes is plotted in Fig.1 as a function of frequency for dielectric height $h_s = 2.1$ mm and permittivity of $\epsilon_r = 12$, and free space height $h = 15$ mm. Furthermore, after calculating the analytical approximations in Eq.4, Newton's method is applied around the approximated solutions to converge closer to the actual value. At frequencies below $f = 10$ GHz (at which the dielectric's height is quarter wavelength), the dominant part of the propagation constant is the imaginary part; also, the imaginary part of the two modes is equal. As the frequency approaches the resonance frequency $f = 9.96$ GHz, the imaginary part becomes smaller and larger deviation between the imaginary parts of the TE1 and TM1 modes is observed. On the other hand, the reverse is observed for the real part - small at frequencies below the resonance frequency, and dominant (and equal for the two modes) at frequencies above the resonance.

The normalized to k_0 propagation constant of the TM1 and TE1 modes is plotted in Fig.6 as a function of the permittivity at a frequency $f = 10$ GHz, dielectric's height $h_s = \lambda_0/4\sqrt{\epsilon_r}$ (quarter-wavelength dielectric), and free space height $h = 15$

mm. As the dielectric's permittivity $\epsilon_r \to 1$, the real and imaginary parts of the modes' propagation constants approach the propagation constant of free space $k_\rho/k_0 \to 1$. However, as the dielectric's permittivity increases, the propagation constants of the two modes become equal and smaller.
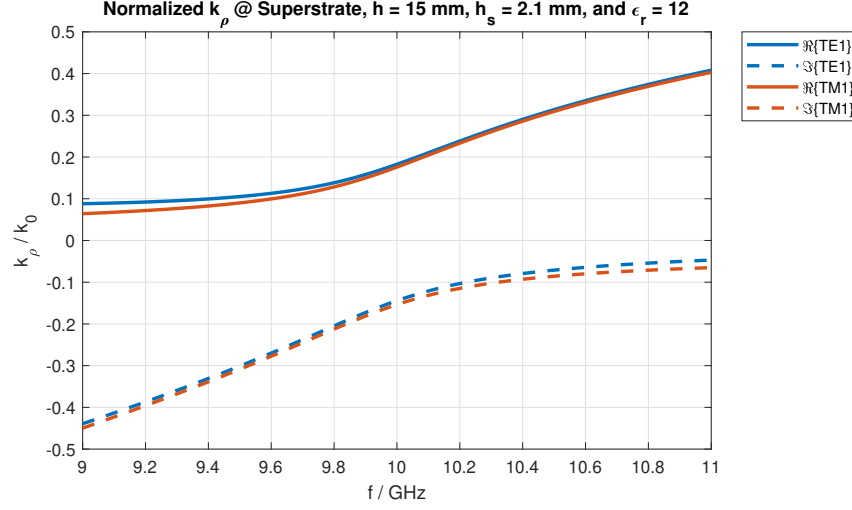

Fig. 1. Propagation constant of the TE1 and TM1 modes normalized to k_0 as a function of the frequency, for a superstrate stratification with free space height $h = 15$ mm, dielectric stub's height $h_s = 2.1$ mm and permittivity $\epsilon_r = 12$.
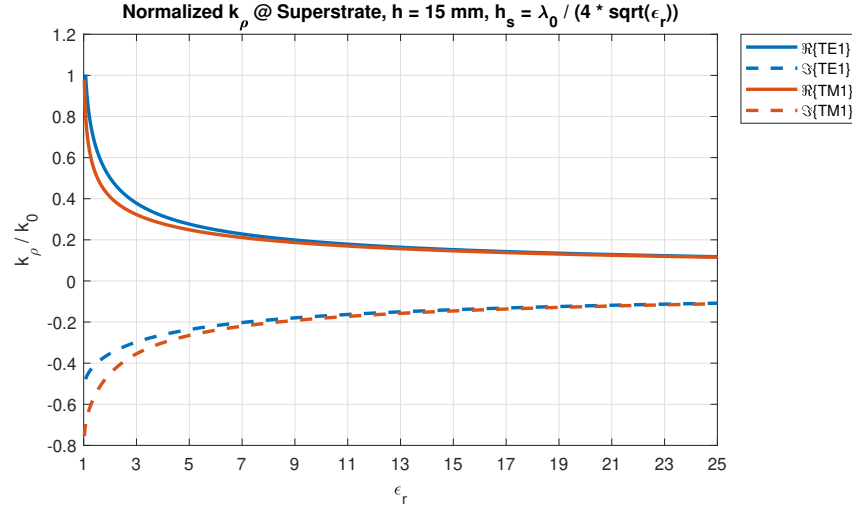

Fig. 2. Propagation constant of the TE1 and TM1 modes normalized to k_0 as a function of the dielectric slab's permittivity, for a superstrate stratification with free space height $h = 15$ mm, dielectric stub's height $h_s = \lambda_0/4\sqrt{\epsilon_r}$, and at a frequency $f = 10$ GHz.

The far-field peaks at the regions close to the leaky wave poles; therefore, changing the poles' locations is used for pattern shaping. Moreover, the saddle points of the far-field are

$$k_{\rho s} = k_0 \sin \theta_s, \tag{5}$$

where θ_s is the elevation angle at the saddle point.

The electric far-field of a magnetic current dipole used in Assignment II[1] (in the $\phi = 0°$ and $180°$, and $\phi = 90°$ and $270°$ planes) is plotted in Fig.3, where the free space height is $h = 5.4$ mm, and the dielectric's height $h_s = 0.77$ mm and permittivity $\epsilon_r = 12$. For a frequency of $f = 30$ GHz, the saddle point is located at $\theta_s = 23.23°$ in $\phi = 0°$, and at $\theta_s = 23.23°$ and $\theta_s = 74.7°$ in $\phi = 90°$. Therefore, leaky waves propagation constants are located near the saddle points at $k_{\rho s}/k_0 = 0.39$ in $\phi = 0°$, and $k_{\rho s}/k_0 = 0.39$ and $k_{\rho s}/k_0 = 0.96$ in $\phi = 90°$ respectively. However, the saddle points represent the regions close to the leaky wave pole locations, where the far-field peaks; the leaky wave propagation constant has also an imaginary components, the poles are branched to the bottom Riemman sheet. Moreover, for a frequency of $f = 28$ GHz, the saddle

---

[1]The electric far-field of the Fabry-Parot antenna discussed during this assignment for frequencies $f = 8, 10, 12$ GHz are plotted in Appendix.A.

points are located at $\theta_s = 7.07°$ in $\phi = 0°$, and at $\theta_s = 7.07°$ and $\theta_s = 74.7°$ in $\phi = 90°$. Finally, for a frequency of $f = 26$ GHz, the saddle points are located at $\theta_s = 73.7°$ in $\phi = 90°$.
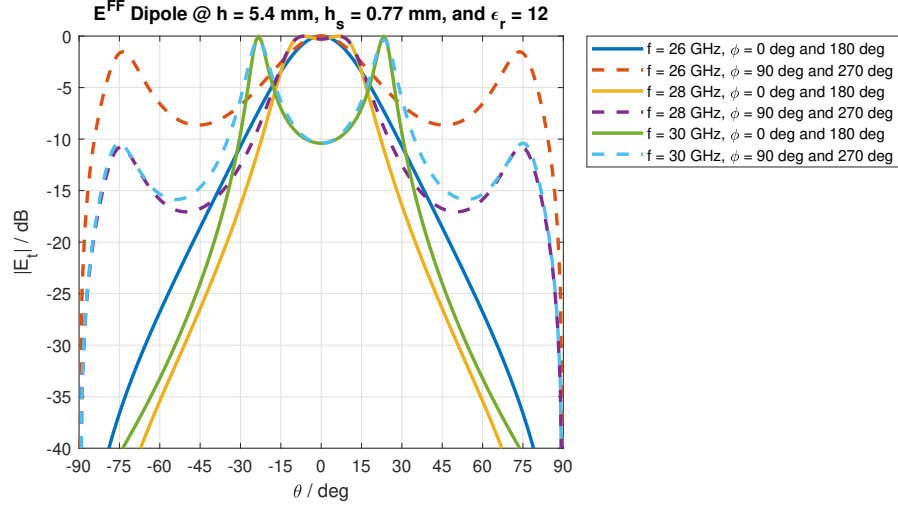

Fig. 3. Electric far-fields of a magnetic current dipole in a superstrate stratification with free space height $h = 5.4$ mm, dielectric stub's height $h_s = 0.77$ mm and permittivity $\epsilon_r = 12$, for frequencies $f = 26,\ 28\ 30$ GHz; the plotted planes are at $\phi = 0°$ and $\phi = 180°$, and $\phi = 90°$ and $270°$ (*assignment II plot*).

The bandwidth is

$$BW = 200 \frac{f_H - f_L}{f_H + f_L},\qquad(6)$$

where f_H and f_L are the -3 dB directivity high and low frequency points respectively. The considered directivity is at broadside, $\theta = 0°$ and $\phi = 0°$. Furthermore, for a quarter-wavelength dielectric, $k_\rho = 0$, therefore, the input impedance seen from the first free space to dielectric interface is

$$Z_L = \frac{\zeta_0}{\epsilon_r}.\qquad(7)$$

As the propagation constant's z-component k_{z0} is dependent on the Z_L, from the analytically derived approximated solution, and the real part of the propagation constant's ρ-component k_ρ is

$$\beta_{LW} = k_0 \sin\theta_{LW},\qquad(8)$$

where θ_{LW} is the angle at which the leaky wave propagates; therefore, a decrease in Z_L (increase in ϵ_r) results in a decrease of θ_{LW}. Hence, for higher permittivity dielectrics, the leaky wave reflects at shorter angles between the dielectric and ground plane. In addition, the relation between the attenuation constant and the dielectric's permittivity is

$$\alpha_{LW} \propto \frac{1}{\epsilon_r},\qquad(9)$$

for both TE1 and TM1 modes. Consequently, increase in the permittivity results in decrease of the attenuation constant. The relation between the effective aperture and the attenuation constant is

$$A_{eff} \propto \frac{1}{\alpha^2}.\qquad(10)$$

Effectively, as the attenuation constant decreases, the leaky wave propagates larger distance, causing an increase in the effective aperture. Therefore, as the effective aperture increases, the directivity also increases. Finally, as the frequency moves away from the resonance, from Eq.8, θ_{LW} increases. Thus, the leaky wave radiates towards directions at large distances from broadside causing a decrease in the broadside directivity. As a summary, increasing the dielectric's permittivity causes a decrease in θ_{LW} and increase in A_{eff} at the resonance frequency of the quarter-wavelength dielectric, resulting in a broadside directivity increase; however, as the frequency moves away from the resonance, θ_{LW} increases, causing a reduction in the broadside directivity, θ_{LW} increases faster with the frequency deviation from the resonance for increasing permittivity, therefore, larger dielectric permittivity results in smaller bandwidth.

The broadside directivity is plotted as a function of frequency for several permittivity values in Fig.4; the free space height is $h = 15$ mm, and dielectric's height $h_s = \lambda_0/4\sqrt{\epsilon_r}$. The simulations correspond to the analytical expectations, as the dielectric's permittivity increases, the resonance also increases and the broadside directivity also increases; however, the bandwidth decreases (the lower and higher -3 dB points move closer to the resonance).

The bandwidth is plotted as a function of the dielectric's permittivity in Fig.5. The simulated results correspond to the analytical expectations, as the permittivity increases, the bandwidth decreases.
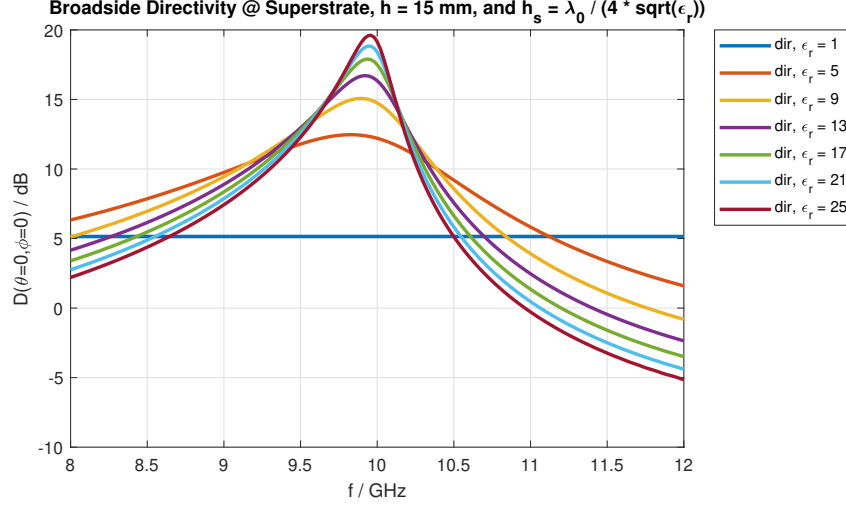

Fig. 4. Directivity, as a function of frequency for several dielectric slab permittivity values, of a Fabry-Parot antenna in a superstrate stratification with free space height $h = 15$ mm and dielectric stub's height $h_s = \lambda_0/4\sqrt{\epsilon_r}$.
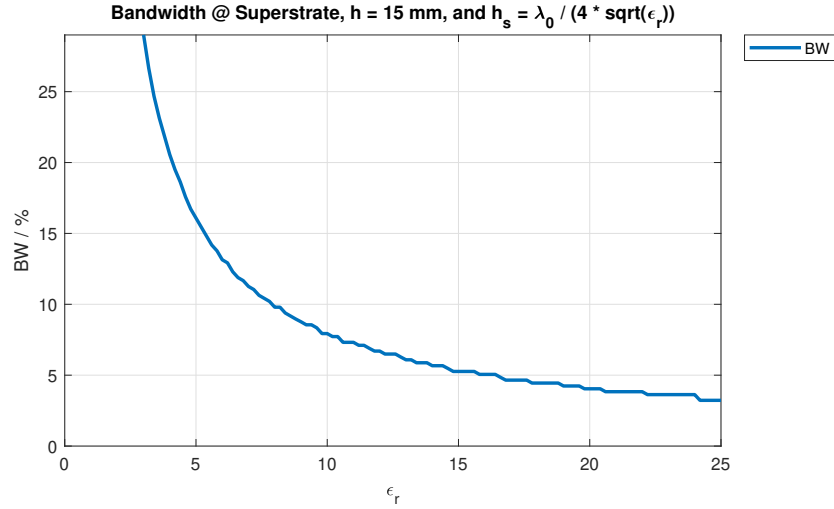

Fig. 5. Bandwidth of a Fabry-Parot antenna, as a function of the dielectric slab's permittivity, in a superstrate stratification with free space height $h = 15$ mm and dielectric stub's height $h_s = \lambda_0/4\sqrt{\epsilon_r}$.

III. SEMI-INFINITE SUPERSTRATE

Similarly to the superstrate, in the semi-infinite superstrate stratification, the dispersion equation is

$$D(k_\rho) = Z_L + j\zeta_0 \tan(k_{z0}h); \tag{11}$$

however, the impedance seen from the free space to dielectric interface is

$$Z_L = \frac{\zeta_0}{\sqrt{\epsilon_r}}. \tag{12}$$

The approximated solutions to the dispersion equation for the TE1 and TM1 modes are

$$k_{z0}^{TE} \approx \frac{k_0}{\pi\sqrt{\epsilon_r}(2\bar{h})^2} \frac{2\pi\bar{h}\sqrt{\epsilon_r} + j}{1 + \frac{1}{(2\pi\bar{h})^2\epsilon_r}}, \tag{13a}$$

$$k_{z0}^{TM} \approx \frac{k_0}{4\bar{h}}(1 + \sqrt{1 + 8j\frac{\bar{h}}{\pi\sqrt{\epsilon_r}}}), \tag{13b}$$

where the approximated solution is in free space (the leaky waves propagate inside the free space medium bounded by the PEC and dielectric). However, the far-field is radiated inside the dielectric layer, thus the z-component of the propagation constant is

$$k_{zd} = j\sqrt{-k_d^2 + k_\rho^2}, \tag{14}$$

where k_d is the propagation constant in the dielectric, and is evaluated in the bottom Riemann sheet.

The normalized to k_d propagation constant of the TM1 and TE1 modes is plotted in Fig.6 as a function of the permittivity at a frequency $f = 15$ GHz and free space height $h = 10$ mm^2. After calculating the approximate solution, Newton's method is applied to converge to its final value. The TE1 and TM1 propagation constants exhibit similar behaviour to the case of the superstrate; however, as ϵ_r increases, the propagation constant converges closer to zero. This effect is due to the impedance seen from the free space to dielectric being smaller by a factor of $1/\sqrt{\epsilon_r}$ compared to superstrate case.
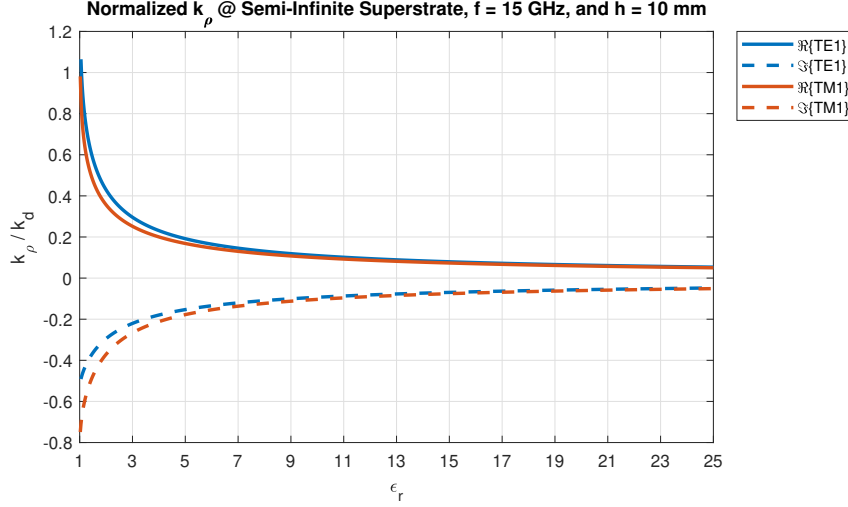

Fig. 6. Propagation constant of the TE1 and TM1 modes normalized to k_d as a function of the dielectric slab's permittivity, for a semi-infinite superstrate stratification with free space height $h = 10$ mm, and at a frequency $f = 15$ GHz.

The directivity of the semi-infinite superstrate is

$$D = 4\pi \frac{A_{eff}\epsilon_r}{\lambda_0^2}; \tag{15}$$

compared to the directivity of the superstrate, $D = 4\pi A_{eff}/\lambda_0^2$, consequently, the semi-infinite superstrate is expected to have ϵ_r higher directivity than the superstrate stratification. This increase in the directivity is the result of the wave propagation inside the dielectric, where the wavelength is smaller, and hence the effective aperture of the antenna increases in terms of the wavelength. Furthermore, due to the smaller Z_L compared to the superstrate stratification, the resonance is expected to be smaller, which results in higher bandwidth than the superstrate case. However, similarly to the superstrate stratification, the bandwidth is expected to decrease as the permittivity increases.

The broadside directivity is plotted as a function of frequency for several permittivity values in Fig.7; the free space height is $h = 10$ mm. The simulations correspond to the analytical expectations. The directivity is higher in the semi-infinite superstrate than the superstrate stratification.

The bandwidth is plotted as a function of the dielectric's permittivity in Fig.8. The simulated results correspond to the analytical expectations. The bandwidth is larger for the semi-infinite superstrate than the bandwidth of the superstrate stratification. And, similarly between the two stratifications, the bandwidth decreases as the permittivity increases.

---

^{2}The propagation constant of the TE1 and TM1 modes as a function of the frequency, as well as the electric far-field of the Fabry-Parot antenna in a semi-infinite superstrate are plotted in Appendix.B.
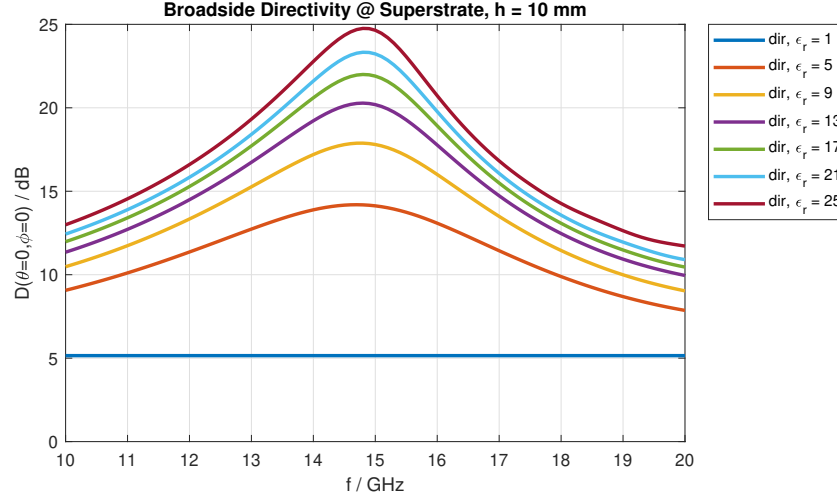
Fig. 7. Directivity, as a function of frequency for several dielectric slab permittivity values, of a Fabry-Parot antenna in a semi-infinite superstrate stratification with free space height $h = 10$ mm.
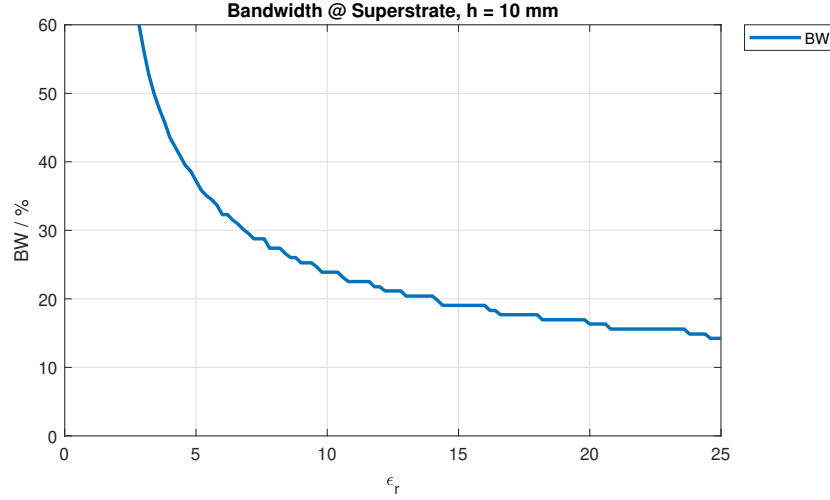

Fig. 8. Bandwidth of a Fabry-Parot antenna, as a function of the dielectric slab's permittivity, in a semi-infinite superstrate stratification with free space height $h = 10$ mm.

IV. SEMI-INFINITE SUPERSTRATE WITH DOUBLE-SLOT ANTENNA

Additionally to the TE1 and TM1 modes, there is a TM0 mode. For a semi-infinite superstrate stratification, the approximate solution is

$$k_{z0}^{TM0} = \sqrt{\frac{jk_0}{\sqrt{\epsilon_r}h}}. \tag{16}$$

The normalized to k_d propagation constant of the TM0 mode is plotted in Fig.9 as a function of frequency; the dielectric layer's permittivity is $\epsilon_r = 10$ and free space height $h = 10$ mm. Over the bandwidth, the TM0 propagation constant does not change.

Two half-wavelength slots are used to cancel the TM0 mode. These slots are at distance d from each other in the x-axis. Therefore, the far-field is

$$E^{FF} \propto 2\cos(\frac{k_x d}{2}), \tag{17}$$

due to the spatial phase difference between the slots (the far-field radiated by each slot has a different phase at the observation points). To cancel the TM0 mode, the TM0 modes excited by two slots must interfere destructively and

$$\cos(\frac{k_{x,LW}d}{2}) = 0, \tag{18}$$

where the x-component of the TM0 propagation constant is equal to the $k_{\rho,LW}$, due to the slots being spaced in the x-axis and hence $\phi = 0°$. Consequently, to cancel the TM0 mode, the slots must be spaced at

$$d = \frac{\pi}{\Re\{k_{\rho,LW}\}}. \tag{19}$$

For a semi-infinite superstrate with dielectric permittivity $\epsilon_r = 10$ and free space height $h = 10$ mm at a frequency $f = 15$ GHz, the spacing between the two double slots must be $d \simeq 10.13$ mm.

The electric far-field of the double slot antenna with slot spacing $d = 10.13$ mm as a function of the elevation angle θ at the planes $\phi = 0°$, $\phi = 45°$, and $\phi = 90°$ is plotted in Fig.10; the semi-infinite superstrate has a dielectric permittivity $\epsilon_r = 10$ and free space height $h = 10$ mm. For comparison the electric far-field of a single slot antenna in the same stratification and at the same planes is plotted in Fig.11. The double slot antenna is more directive at broadside. The saddle point at $\theta = 18.16°$ and $\phi = 0°$ is removed and a null occurs instead (hence, it can be concluded that the far-field peak at $\phi = 0°$ is associated with the TM0 mode). Furthermore, the peak (saddle point) at $\phi = 45°$ is reduced compared to the single slot.

The directivity of the double slot antenna with slot spacing $d = 10.13$ mm as a function of the elevation angle in the same stratification and at the same planes is plotted in Fig.12. The maximum directivity is at broadside with 22.67 dB.
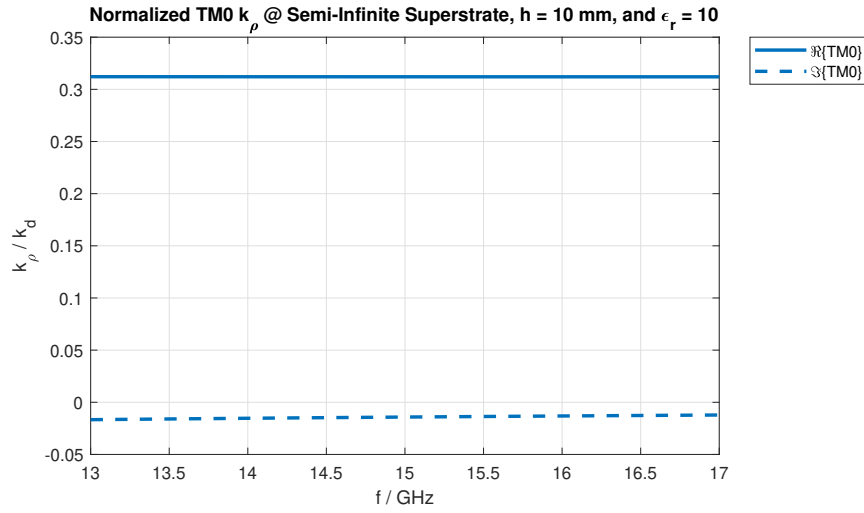

Fig. 9. Propagation constant of the TM0 modes normalized to k_d as a function of the frequency, for a semi-infinite superstrate stratification with free space height $h = 10$ mm, and dielectric stub's permittivity $\epsilon_r = 10$.
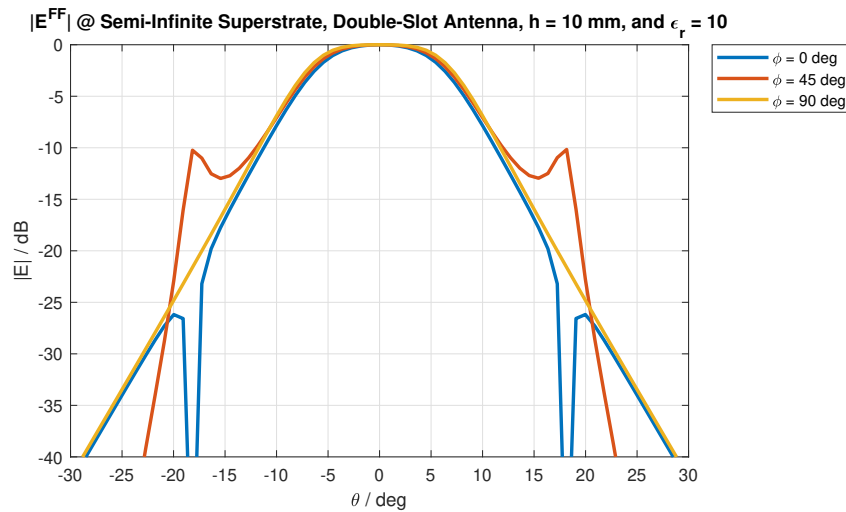

Fig. 10. Electric far-field of a double slot antenna, the spacing between the slots is such that the TM0 mode is cancelled, in a semi-infinite superstrate with free space height $h = 10$ mm and dielectric slab's permittivity $\epsilon_r = 10$; the plotted planes are $\phi = 0°$, $\phi = 45°$, and $\phi = 90°$.

|E^{FF}| @ Semi-Infinite Superstrate, Single-Slot Antenna, h = 10 mm, and ϵ_r = 10
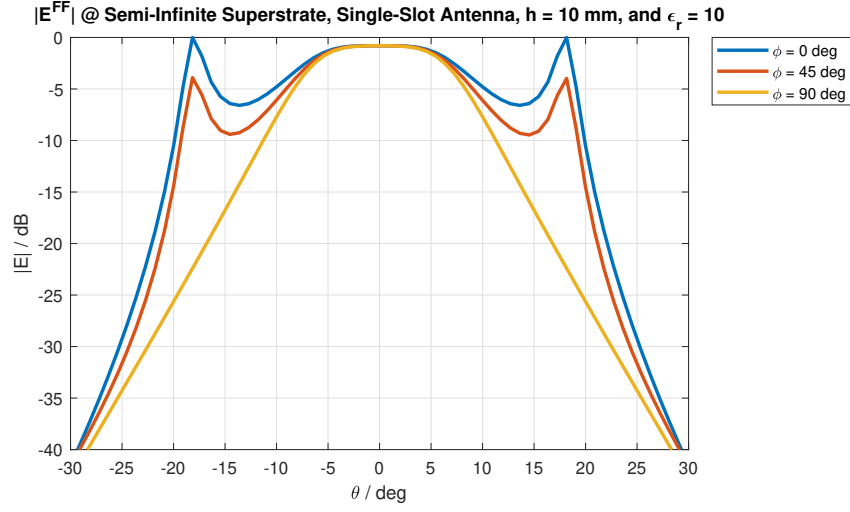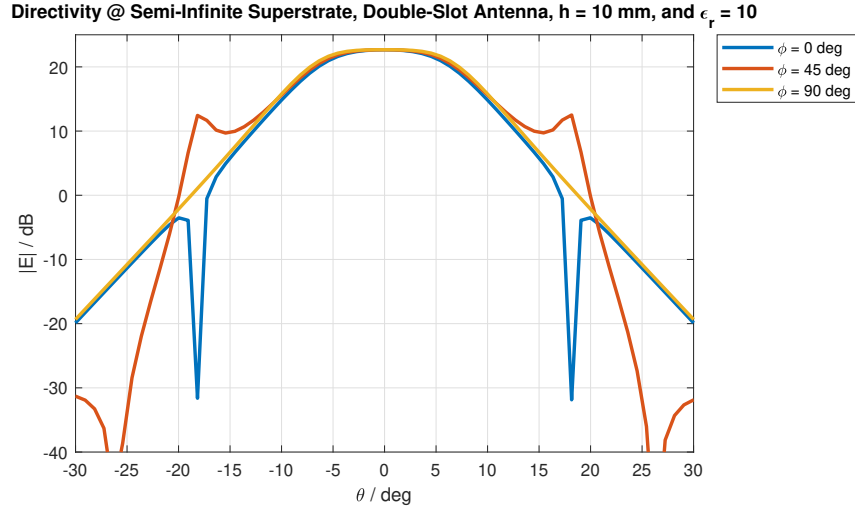

Fig. 11. Electric far-field of a single slot antenna in a semi-infinite superstrate with free space height $h = 10$ mm and dielectric slab's permittivity $\epsilon_r = 10$; the plotted planes are $\phi = 0°$, $\phi = 45°$, and $\phi = 90°$.

Directivity @ Semi-Infinite Superstrate, Double-Slot Antenna, h = 10 mm, and ϵ_r = 10

Fig. 12. Directivity of a double slot antenna, the spacing between the slots is such that the TM0 mode is cancelled, in a semi-infinite superstrate with free space height $h = 10$ mm and dielectric slab's permittivity $\epsilon_r = 10$; the plotted planes are $\phi = 0°$, $\phi = 45°$, and $\phi = 90°$.

APPENDIX A
ADDITIONAL SUPERSTRATE PLOTS

E Far-Field @ Superstrate, h = 15 mm, h$_s$ = λ_0 / (4 * sqrt(ϵ_r)), and ϵ_r = 25
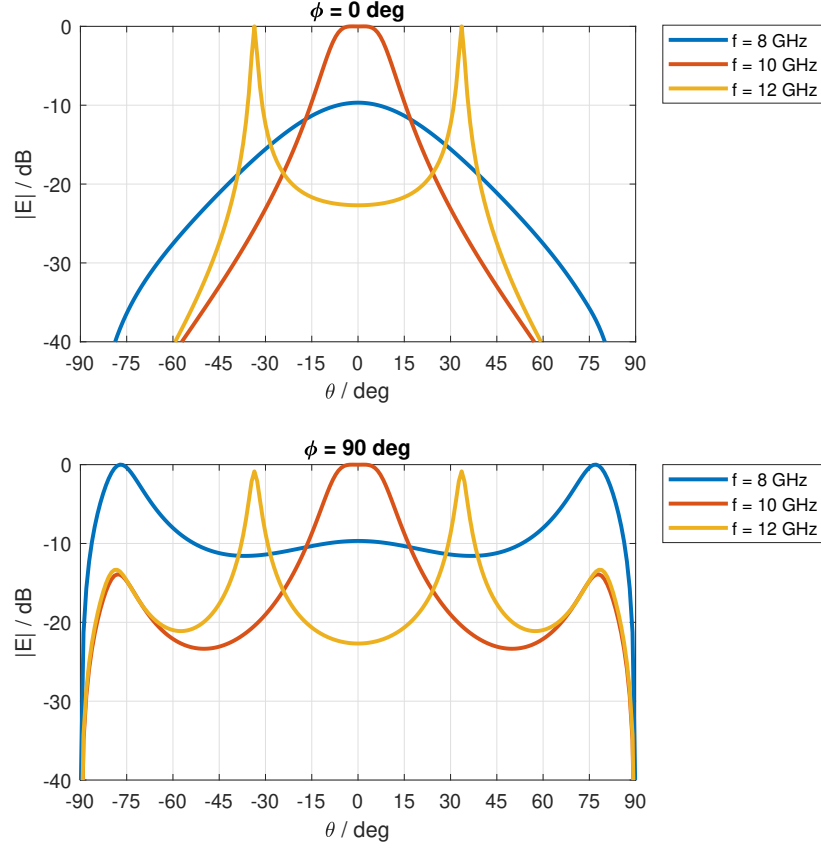

Fig. 13. Electric far-fields of a Fabry-Parot antenna in a superstrate stratification with free space height $h = 15$ mm, dielectric slab's height $h_s = \lambda_0/4\sqrt{\epsilon_r}$ and permittivity $\epsilon_r = 25$; the plotted planes are $\phi = 0°$ and $180°$, and $\phi = 90°$ and $270°$.

APPENDIX B
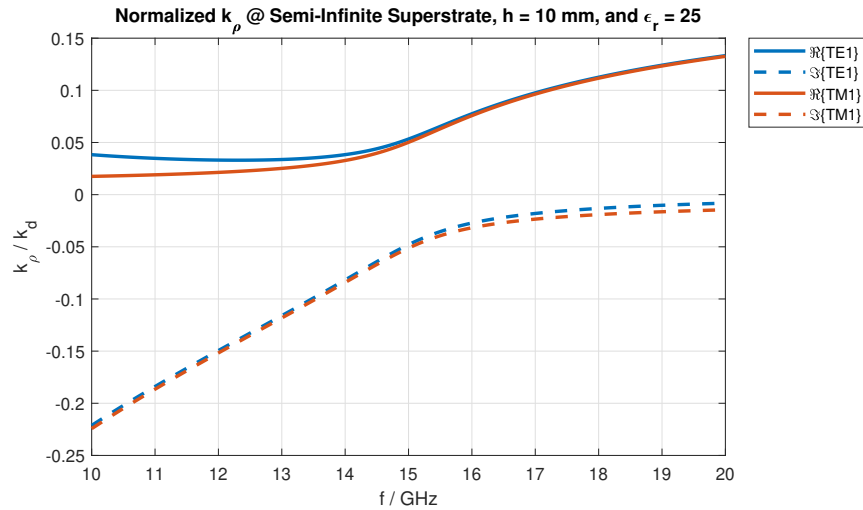## ADDITIONAL SEMI-INFINITE SUPERSTRATE PLOTS

Fig. 14. Propagation constant of the TE1 and TM1 modes normalized to k_d as a function of the frequency, for a semi-infinite superstrate stratification with free space height $h = 10$ mm, and dielectric stub's permittivity $\epsilon_r = 25$.
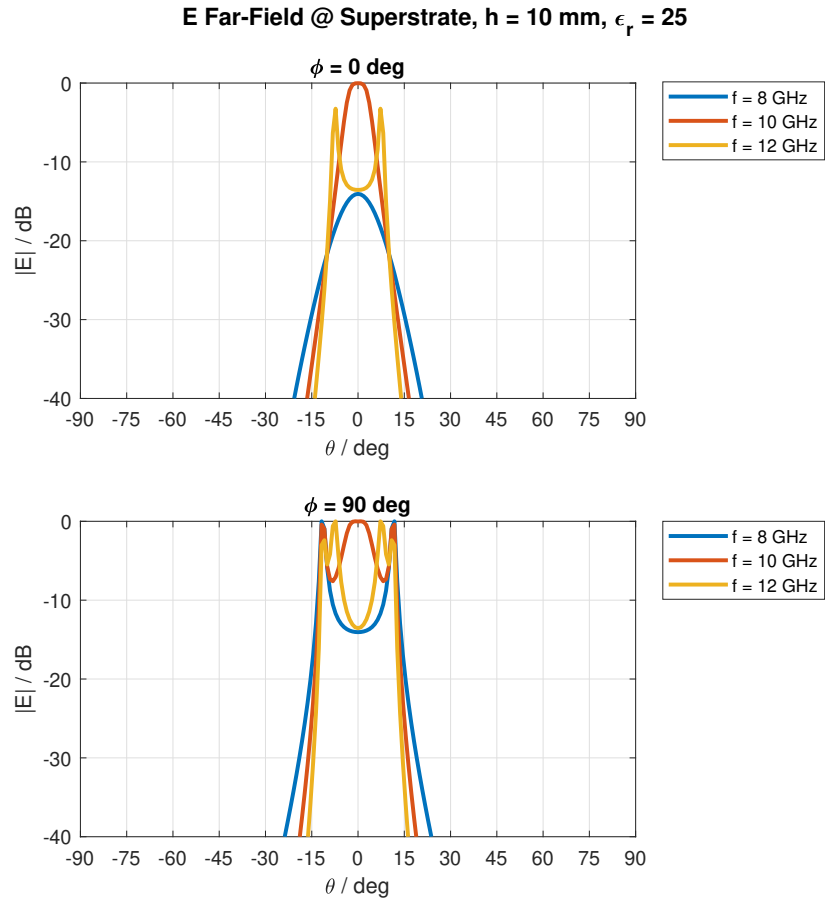
Fig. 15. Electric far-fields of a Fabry-Parot antenna in a semi-infinite superstrate stratification with free space height $h = 10$ mm, and dielectric slab's permittivity $\epsilon_r = 25$; the plotted planes are $\phi = 0°$ and $180°$, and $\phi = 90°$ and $270°$.